ELSEVIER

Biochimica et Biophysica Acta 1273 (1996) 175–190

BBA Biochimica et Biophysica Acta

Exciton equilibration and Photosystem II exciton dynamics – a fluorescence study on Photosystem II membrane particles of spinach

Holger Dau [*,1], Kenneth Sauer

Department of Chemistry and Structural Biology Division, Lawrence Berkeley Laboratory, University of California, Berkeley, CA 97420, USA

Received 6 April 1995; revised 24 July 1995; accepted 11 October 1995

Abstract

The Photosystem II (PS II) exciton dynamics at room temperature was investigated by steady-state and picosecond fluorescence measurements on PS II membrane particles of spinach. In the closed as well as in the open-reaction center state, emission and excitation spectra were found to be almost independent of the excitation (λ_{ex}) and emission wavelength (λ_{em}), respectively. This holds even for anti-Stokes spectra ($\lambda_{em} < \lambda_{ex}$). The minor differences observed are suggestive of excitation energy transfer from short-wavelength forms of chlorophyll (Chl) to long-wavelength Chl. The relation between the emission spectrum and the excitation spectrum of the PS II antenna system is well described by the Stepanov relation (Sov. Phys. Dokl. 2 (1957) 81–84) originally derived for a single pigment in thermal equilibrium with its environment. The picosecond fluorescence decays measured at various emission wavelengths were described in terms of four exponential lifetime components with common time constants. For Chl *b* excitation at 645 nm, the amplitude of the fastest decay component is negative for $\lambda_{em} > 690$ nm indicating excitation energy transfer with a time constant of 15 ps. A model for the PS II exciton dynamics in the open reaction center state is proposed which describes the fluorescence relaxation in terms of three phases: (I) ultra-fast exciton equilibration (time constants < 15 ps) within a peripheral pigment pool consisting of LHC pigments and within an inner pigment pool presumably consisting of PS II core pigments, (II) rapid exciton equilibration (time constant of 15 ps) between these two pigment pools and (III) excited state decay by primary charge separation according to the reversible radical pair model (time constants of 131 ps and 322 ps), but maintenance of the exciton equilibrium distribution. Because the equilibration time of 15 ps is fast in comparison to the mean exciton lifetime of 220 ps, the steady-state fluorescence properties are determined mainly by the thermal equilibrium distribution of excited states on the PS II chlorophylls (Chl *a* and Chl *b*).

Keywords: Chlorophyll; Excitation energy transfer; Kinetic model; Photosynthesis; Picosecond fluorescence; Primary charge separation; Thermal equilibrium

1. Introduction

The Photosystem II holocomplex of higher plants and green algae contains 200–300 chlorophyll molecules (~ 65% Chl *a* and ~ 35% Chl *b*) and various carotenoids which are non-covalently bound to various PS II polypeptides [1,2]. By absorption of a photon, either a single PS II-pigment reaches an excited state, or a group (two or more) of excitonically coupled pigments becomes coherently excited (strong coupling limit). The excited singlet state of a PS II pigment may relax to the singlet ground state under simultaneous excitation of a neighboring pigment, a process often discussed as the movement or 'hopping' of an 'exciton' from donor to acceptor pigment [3]. A theoretical description was first derived by Förster [4,5]. After several hopping steps the exciton may reach the reaction center pigment, P680, where the excited-state energy of $P680^*$ can be used to drive the primary charge separation reaction, i.e., the formation of the primary radical pair [$P680^+$, $Pheo^-$].

The PS II chlorophylls are heterogeneous in their spectroscopic properties. A deconvolution of Q_y absorption and fluorescence emission spectra into Gaussian compo-

Abbreviations: Chl, chlorophyll; CP, chlorophyll protein complex; DCBQ, 2,6-dichloro-1,4-benzoquinone; F_M, fluorescence with reduced Q_A; F_0, fluorescence with oxidized Q_A; fwhm, full-width at half-maximum; LHC, light-harvesting complex; LHCII, *lhcb1* and *lhcb2* gene products; Mes, 4-morpholinoethanesulfonic acid; Pheo, a special pheophytin acting as the primary electron acceptor; PS, Photosystem; Q_A, a special plastoquinone acting as the secondary electron acceptor.

* Corresponding author (at permanent address). Fax: +49 6421 282057; e-mail: dauh@mailer.uni-marburg.de.

[1] Permanent address: FB Biologie/Botanik, Philipps-Universität, D-35032 Marburg, Germany.

SSDI 0005-2728(95)00141-7

nents reveals the existence of at least six spectral species: P_{648}^{653}, P_{660}^{663}, P_{670}^{672}, P_{678}^{680}, P_{684}^{687}, P_{695}^{697} (P_a^e denotes the chorophyll species absorbing maximally at a nm and emitting maximally at e nm, deconvolution of Zucchelli et al. [6]). Likewise, the PS II polypeptides are characterized by a considerable diversity: about 20 mostly non-identical pigment-protein complexes are part of a single PS II (10 dissimilar gene products [7]). All spectral types of Chl a were found to be present in all PS II pigment-protein complexes; long-wavelength chlorophylls (absorption maximum at higher wavelengths than the P680 absorption) seem to be enriched in the polypeptides close to the PS II reaction center complex [6,8]. The pigments are tightly packed within a single polypetide (Mg to Mg distance of 10 to 14 Å between neighboring LHC chlorophylls), but not in the form of a regular lattice [9,10].

The kinetics of PS II exciton movement and trapping have been subject of numerous investigations; for recent reviews see [11–14]. Hodges and Moya [15] studied the picosecond fluorescence kinetics of PS II membrane particles. For fully dark-adapted PS II, they resolved three lifetime components of 20 ps, 150 ps and 350 ps; Van Mieghem et al. [16] found lifetime components of 140 ps and 330 ps. In both articles, decay-associated spectra were not presented.

Based on simulations Laible et al. [17] concluded that following light absorption a quasi-equilibrium state is reached within 10–30 ps. We present new experimental results, and we discuss to what extent the fluorescence properties of the intricate PS II pigment system can be understood by using equilibrium thermodynamics. In particular, it is investigated whether 'rapid exciton equilibration' occurs [18–21]. Therefore, definitions of 'exciton equilibrium' and 'rapid exciton equilibration' are first given. Based on these definitions, experimentally testable criteria for 'rapid exciton equilibration' are derived. And indeed, the experimental results of this study indicate that the PS II fluorescence properties are determined by 'rapid exciton equilibration'. Finally, we consider the equilibration process itself and a model for the PS II exciton dynamics is proposed, which is an extension of the reversible radical pair (RRP) model [18,22].

2. Materials and methods

2.1. PS II particles

Oxygen-evolving PS II membrane particles were prepared by solubilization of broken spinach chloroplasts with Triton X-100 followed by three washing steps as described in [23].

For the resulting PS II membrane particles, the rates of oxygen evolution at saturating light intensities (assay buffer: 50 mM NaCl, 2 mM $MgCl_2$, 3.5 mM ferricyanide, 250 μM DCBQ, 20 mM Mes (pH 6.0)) were between 350 and 500 μmol O_2/mg Chl per h. The Chl a to Chl b ratio was 1.9 ± 0.1 (w/w). The ratio between the fluorescence yield of PS II particles with light-reduced primary quinone acceptor (F_M) and the fluorescence yield of the dark-adapted PS II particles (F_o) was between 3.5 and 4.5. At 77 K, the fluorescence emission peak at 695 nm (F_{695}, PS II emission, hardly any PS I contribution) was 4-times higher than the fluorescence emission peak at 735 nm (F_{735}, PS II and PS I emission). Based on the low-temperature fluorescence data, we estimate the PS I content of the PS II preparation to be less than 3%. (For this rough estimate it was assumed: F_{695}/F_{735} of broken chloroplasts ~ 0.3, PS II to PS I stoichiometry of broken chloroplasts ~ 2, F_{695}/F_{735} ratio of a pure PS II preparation ~ 8.)

2.2. Fluorescence measurements

For fluorescence measurements, the PS II preparations were diluted in 50 mM Mes (pH 6.0)/15 mM NaCl/5 mM $MgCl_2$/5 mM $CaCl_2$/400 mM sucrose to a final Chl concentration of 10 μg/mL. Steady-state and time-resolved fluorescence measurements were made at room temperature using a flow system with a fluorimeter flow cell of square cross-section (2×2 mm) as described in [24].

For measurements in the F_0 state (dark-adapted state, open-RC state without reduced Q_A), the PS II preparation was rapidly pumped from the bottom of the sample reservoir through the fluorimeter flow cell and back to the top of the sample reservoir. The large reservoir volume of 250 mL ensured full dark-adaptation. Lengthening the exchange time for the light-exposed volume of the flow-cell from 50 ms to 100 ms (by decreasing the flow rate) did not result in any detectable increase of the fluorescence emission. This indicates that the exposure to the measuring light did not result in significant PS II trap closure by the light-induced reduction of some PS II quinone acceptors.

After stopping the pump, the level of the chlorophyll fluorescence emission increased by a factor of 3.5 to 4.5 within a few seconds. The fluorescence yield and spectra of the high-fluorescent state obtained by stopping the pump remained constant for at least 10 min. This high-fluorescent state, which results from the light-induced reduction of the primary quinone acceptor (Q_A) upon prolonged illumination, is denoted as 'F_M state' in the following.

For steady-state fluorescence measurements a fluorometer (SPEX Fluorolog 2 model 212) equipped with double monochromators for selection of excitation wavelengths and emission wavelengths was used. Usually, excitation and emission monochromators slits were set to 1 mm resulting in a half-maximum bandwidth of about 1.8 nm. For excitation at 695 nm, the excitation monochromator slits were set to 2 mm in order to obtain a photon flux which guarantees complete trap closure for F_M-state spectra. Data were collected in 1 nm steps with a dwell-time of typically 5 s per data point. Single-photon counting detec-

tion was employed. Whenever the count-rate of the sample was lower than 100-times the dark-count rate, the dark-count rate was subtracted. Excitation and emission spectra, which were recorded with right-angle fluorescence detection, were corrected for the spectral characteristics of the excitation and detection system, respectively.

Picosecond fluorescence measurements were carried out at room temperature (25–28°C) by time-correlated single-photon counting using the experimental set-up described elsewhere [25,26]. Fluorescence decays were detected at different wavelengths with monochromator slits corresponding to approximately 4 nm fwhm. The channel width for the time-resolved measurements was 5.8 ps. The instrument response function was determined using a light-scattering suspension; the half-maximum full-width duration was 55–65 ps. For each decay, 5000 or 10 000 counts were collected at the peak channel.

By curve-fitting, employing iterative deconvolution with the instrument response function, all fluorescence decay data were resolved into a sum of exponentials described by the pre-exponential factors A_i (in the following called 'amplitudes') and the time constants T_i with T_1 labeling the fastest lifetime component. For Fig. 4B, the relative yield, Y_i, of lifetime component i was calculated according to: $Y_i = A_i T_i / \Sigma A_j T_j$. The fit results shown in Fig. 4 were obtained by so-called 'global data analysis' [27,28]. This technique involves the simultaneous fit of decays measured at different emission wavelengths under the constraint of an identical set of time constants for all emission wavelengths, i.e., the time constants are required to be wavelength independent.

3. Results

First we will give explicit definitions for 'exciton equilibrium' and 'rapid exciton equilibration'. For this purpose, the following assumptions are made.

The phrase 'an exciton resides on Chl_i' denotes a situation where one distinct chlorophyll (Chl_i) is in an excited state and all other chlorophylls are in their ground state; excitation energy transfer is described as the movement of these localized excitons. After vibrational relaxation of the initially excited state, which occurs within clearly less than 10 ps, excitation energy transfer (exciton hopping) from Chl_l to Chl_m is describable by the first order rate constant k_{lm} (Markoffian approximation, see [3]). Each Chl_i is characterized by a a distinct energy, E_i (in the following often denoted as site energy) such that for any pair of chlorophylls the following relation holds (k, Boltzmann constant; T, temperature in K)

$$k_{lm}/k_{ml} = e^{-(E_m - E_l)/kT} \quad (1)$$

It should be noted that the energy difference in Eq. (1) (i.e., $E_l - E_m$) is not necessarily comparable to the difference in energies of the respective electronic transitions from the ground state to the first excited singlet state. Rather than being the energy of the electronic transition, E_i is the free energy of the following state: Chl_i is in an excited state and all other pigments of the antenna system are in their ground state. Nonetheless, in many cases a reasonable estimate for E_i should be obtainable from the wavelength of the Chl_i absorption maxima, λ_i, according to: $E_i = hc/\lambda_i$ with h and c being the Planck constant and velocity of light, respectively.

We will call an 'exciton equilibrium' a state where the probability p_i for the excited state to reside on Chl_i is approximately proportional to the Boltzmann factor: $e^{-E_i/kT}$. Thus, for an exciton equilibrium the relative residence probability, p_i, is given by

$$p_i = c_i \frac{e^{-E_i/kT}}{\sum_j c_j e^{-E_j/kT}} \quad (2)$$

for any pigment of the antenna system. In Eq. (2), c_i is a time-independent factor which should be close to one for an exciton equilibrium.

The exciton equilibrium as defined above is characterized by an excited state distribution which is close to a thermodynamic equilibrium distribution. Assuming the validity of the above-mentioned assumptions (Eq. (1)), a perfect Boltzmann distribution would be obtained in the absence of any excited state decay (excited state decay due to primary charge separation, non-radiative transitions to the ground state and fluorescence emission). However, because in the real photosystem excited state decay occurs, deviations from a perfect Boltzmann distribution are inevitable. The factor c_i accounts for these deviations. For an ideal Boltzmann distribution, c_i is equal to 1.0; due to the quasi-equilibrium character deviations from unity occur. We consider a value c_i between 0.9 and 1.1 to be sufficient to justify the use of the term 'exciton equilibrium'.

The mean exciton lifetime, τ_{mean}, is defined by (other definitions are possible, e.g., in [14])

$$\tau_{mean} = \int_0^\infty P_A(t)dt / P_A(0) \quad (3)$$

where $P_A(t)$ gives the probability that after delta-pulse excitation (at $t = 0$) one pigment of an individual PS II antenna system is in its excited state.

For pulsed excitation, establishment of an exciton equilibrium usually occurs with complex kinetics, the 'equilibration kinetics'. We will use the term 'rapid exciton equilibration' if the slowest time constant involved in the exciton equilibration kinetics, τ_{eq}, is small in comparison to the mean exciton lifetime, τ_{mean}:

$$\tau_{eq} < \tau_{mean} \quad (4)$$

The hypothetical case of $\tau_{eq} = 0$ is called 'perfectly rapid exciton equilibration'.

For pulsed excitation, after exciton equilibration has taken place the fluorescence emission spectrum of a large PS II ensemble, $F_A^{em}(\lambda_{em})$, is determined by the emission spectra of the individual pigments, F_i^{em}, weighted with the relative residence probability, p_i; i.e.,

$$F_A^{em}(\lambda_{em}) = \Sigma\{p_i \cdot F_i^{em}(\lambda_{em})\}. \quad (5)$$

Obviously, the shape of the emission spectrum as determined by Eq. (5) does not depend on the wavelength used for excitation; the amplitude of the spectrum should be proportional to the number of excitons created by light absorption, i.e., it should be proportional to the extinction coefficient, $\epsilon(\lambda_{ex})$. Furthermore, the spectra are time-independent; at all emission wavelengths the fluorescence relaxation kinetics is determined by the same function, $P_A(t)$. In summary, after exciton equilibration has taken place, the fluorescence emission, $F(\lambda_{em}, \lambda_{ex}, t)$, is described by the following equation:

$$F_i(\lambda_{em}, \lambda_{ex}, t) = \epsilon(\lambda_{ex}) \cdot P_A(t) \cdot F_A^{em}(\lambda_{em}). \quad (6)$$

For perfectly rapid exciton equilibration ($\tau_{eq} = 0$), the fluorescence emission detected by using a continuous measuring light (steady-state fluorescence) is given by

$$F(\lambda_{em}, \lambda_{ex}) = \epsilon(\lambda_{ex}) \cdot F_A^{em}(\lambda_{em}) \cdot \tau_{mean}. \quad (7)$$

Eqs. (2)–(7) provide criteria for the case of 'rapid exciton equilibration', which makes the hypothesis of rapid exciton equilibration within the PS II antenna system testable. (However, the experimental test will be almost certainly misleading if sample heterogeneities are not fully insignificant.) For rapid exciton equilibration the following must be valid with only minor deviations: (1) the steady-state emission spectra are independent of the excitation wavelength; (2) the steady-state excitation spectra are independent of the wavelength used for detection of fluorescence; (3) trap closure does not affect the form of emission or excitation spectra; (4) the emission spectrum reflects the equilibrium distribution of the excited state residence probability according to Eq. (2) and Eq. (5); (5) for picosecond fluorescence relaxation measurements, there are no changes in the spectra for times $t \gg \tau_{eq}$; (6) the time constants for risetimes detected by fluorescence relaxation measurements are small in comparison to the mean lifetime. In the following, the validity of these criteria is tested.

To verify the excitation-wavelength independence of the PS II emission spectra, emission spectra were collected for various excitation wavelengths in the F_0 state and in the F_M state. In Fig. 1, F_M state emission spectra for excitation at 620 nm (lowest-lying thin line), 695 nm (top thin line), 677 nm (closed triangles) and 645 nm (intermediate thin line) are shown.

Light of the selected excitation wavelengths is assumed to excite different classes of PS II chlorophylls:

(a) At 620 nm, presumably all Chl *a* of the PS II antenna are absorbing. For excitation at 620 nm, there is no overlap between excitation wavelength and the emission spectrum. Therefore, the complete emission spectrum was detectable. This emission spectrum is shown for wavelengths to 705 nm in Fig. 1. In contrast, for other excitation wavelengths only limited regions of the spectra are shown (in Figs. 1 and 2) which are not significantly influenced by contributions from scattering of the excitation light.

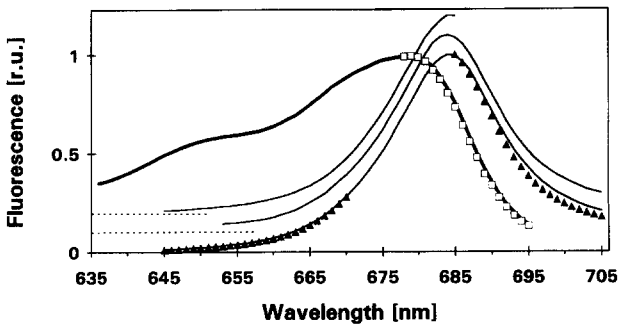

Fig. 1. Fluorescence excitation and emission spectra of PS II particles at room temperature. The thick line and the open squares give excitation spectra obtained by fluorescence detection at 760 nm (Stokes fluorescence) and 665 nm (anti-Stokes fluorescence), respectively. The three thin lines and the closed triangles give emission spectra for various excitation wavelengths: top line, 695 nm excitation; intermediate line, 645 nm excitation; lowest line, 620 nm excitation; closed triangles, 677 nm excitation. All spectra were collected in the F_M state and normalized to 1.0 at the excitation or emission peak. The normalized emission spectra for 645 nm and 695 nm excitation are shifted upwards by 0.1 and 0.2 units, respectively; the resulting zero levels are indicated by broken lines.

(b) At 645 nm, Chl *b* molecules of the LHCs are predominantly absorbing. Thus, PS II chlorophylls with the highest S_1 energy and perhaps the most distant location with respect to the reaction center are (initially) excited.

(c) At 695 nm, the long-wavelength chlorophylls (lowest S_1 energy) are absorbing. The fluorescence emission was detected at wavelengths shorter than the excitation wavelength ('anti-Stokes fluorescence'). Presumably, the anti-Stokes fluorescence detected is due to fluorescence decays occurring after thermally activated excitation energy transfer from long-wavelength to short-wavelength chlorophylls.

(d) At 677 nm, the excitation occurs at the center of the PS II-Chl *a* absorption peak. Thus, the dominant class of the Chl *a* molecules is initially excited. Stokes fluorescence and anti-Stokes fluorescence were detectable.

As shown in Fig. 1, different excitation wavelengths result in almost identical emission spectra. The same holds for PS II in the F_0 state. Likewise, the shape of the excitation spectrum was found to be almost independent of the wavelength used for detection of fluorescence. This holds also for the excitation spectrum of the anti-Stokes fluorescence detected at 665 nm (open squares in Fig. 1).

The presence of small differences between emission spectra obtained with different excitation wavelengths, however, is obvious in the F_0-state ratio spectra shown in Fig. 2E, F. In Fig. 2, all spectra were normalized to a value

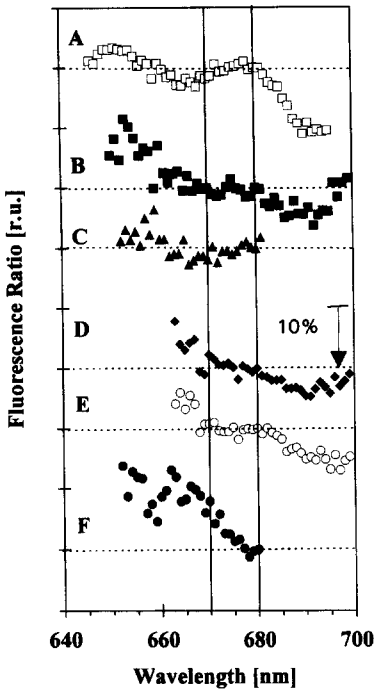

Fig. 2. Influence of excitation wavelength on emission spectra and effect of quenching by open reaction centers on the fluorescence spectra of PS II particles. Excitation and emission spectra were measured either in the open RC state (F_0 fluorescence) or in the closed RC state (F_M fluorescence). All spectra were normalized to 1.0 at 680 nm and for each wavelength the ratio of the normalized fluorescence was calculated. For [A]–[F], the broken line corresponds to a ratio of 1.0; the arrow length (identical to the distance between y-axis tick marks) indicates a deviation of the fluorescence ratio from unity by 10%. The following fluorescence ratios are shown: [A] (F_0/F_M) versus excitation wavelength for fluorescence detection at 760 nm; [B] (F_0/F_M) versus emission wavelength for excitation at 475 nm; [C] (F_0/F_M) versus emission wavelength for excitation at 695 nm; [D] (F_0/F_M) versus emission wavelength for excitation at 645 nm; [E] (F_0 for excitation at 645 nm/F_0 for excitation at 620 nm) versus emission wavelength; [F] (F_0 for excitation at 620 nm/F_0 for excitation at 695 nm) versus emission wavelength.

of 1.0 at 680 nm before ratios were calculated. The ratio spectra are used to demonstrate the presence of small differences in the shape of the steady-state spectra. The differences in the shape of the normalized spectra are given in percent (for details see legend of Fig. 2).

Upon excitation of Chl *b* at 645 nm (Fig. 2E), the emission of short wavelength chlorophylls (emission at about 665 nm) is enhanced by ~ 5% with respect to the fluorescence emission measured upon excitation of Chl *a* at 620 nm; the emission of long-wavelength chlorophylls (emission at about 695 nm) is diminished by about 5%. Note that 0% enhancement at 680 nm results from the normalization at 680 nm.

For excitation of Chl *a* molecules at 620 nm (Fig. 2F) the short-wavelength emission is enhanced with respect to the anti-Stokes fluorescence emission obtained by specific excitation of long-wavelength chlorophylls at 695 nm.

There are no pronounced differences between the emission or excitation spectra of PS II in the closed reaction center state (F_M state, spectra shown in Fig. 1) and in the open reaction center state (F_0, spectra not shown). Thus, fluorescence quenching by open reaction centers does not result in major modifications of excitation or emission spectra. However, there are some minor differences as shown in Fig. 2A–E. These differences resemble effects described by Jennings et al. [29,30]. (For the anti-Stokes ratio spectrum shown in Fig. 2C and 2F, the fluorescence ratios between 670 nm and 680 nm could be affected by light-scattering artefacts. The reason is that only for excitation at 695 nm was a relatively large excitation monochromator bandwidth of ~ 3.6 nm used to achieve photon flux densities sufficient for complete trap closure.)

For rapid exciton equilibration, Eqs. (2) and (5) predict that the steady-state emission spectrum is given by the Boltzmann-weighted sum of the pigment emission spectra. Verification of the relation predicted by Eq. (2) was approached by investigating the validity of the Stepanov relation [31,32].

In the case of PS II, the system under consideration is a large cluster of pigments with considerable inhomogeneous broadening of spectral bands and excitation energy transfer between pigments. The Stepanov relation was derived to relate absorption and emission spectra of dye molecules in the absence of inhomogeneous broadening and excitation energy transfer [31,32]. Thus, the Stepanov relation in its original formulation is not applicable for analysis of the PS II antenna system. A basic assumption for the derivation of the Stepanov relation has been that a thermal equilibrium population of vibronic sublevels is rapidly established after the absorption event. If this assumption is extended to include rapid equilibration among all excited-state energy levels of different pigments of one pigment cluster, we obtain a relation which is formally identical to the relation originally derived by Stepanov, i.e.

$$h\nu \cdot F(\nu) = D(T) \cdot \{(8\pi h \nu^3)/c^3\} \cdot \epsilon(\nu) \cdot e^{-h\nu/(kT)} \quad (8)$$

with: $F(\nu)$, spectral density of the fluorescence quantum yield of the pigment system per unit frequency interval; $\epsilon(\nu)$, extinction of the pigment system; $D(T)$, temperature-dependent factor which is independent of ν; h, Planck constant; c, light velocity; k, Boltzmann constant.

Rapid exciton equilibration implies that the absorption spectrum, $\epsilon(\nu)$, is identical to the fluorescence excitation spectrum, $F^{ex-sp}(\nu)$, detected at (infinitesimally) low sample concentrations. For testing the validity of Eq. (8) we decided to use $F^{ex-sp}(\nu)$ instead of $\epsilon(\nu)$. There are two advantages in using the excitation spectrum: (1) light scattering, which could seriously affect $\epsilon(\nu)$, will barely affect $F^{ex-sp}(\nu)$, and (2) distortion of the fluorescence emission spectrum, $F^{em-sp}(\nu)$, due to fluorescence reabsorption will not affect the ratio between $F^{em-sp}(\nu)$ and $F^{ex-sp}(\nu)$ significantly as discussed in the following.

Only for extremely low sample concentrations should the excitation spectrum closely resemble exactly the absorption spectrum. We estimate that for Chl concentrations of 10 μg/mL and a optical path of 2 mm the deviations between absorption and excitation spectra might be as high as 15% at the absorption peak. The fluorescence emission spectra are distorted by fluorescence reabsorption. The ratio $F^{em-sp}(\nu)/F^{ex-sp}(\nu)$, however, is not affected because the distortions of emission spectrum and excitation spectrum will largely compensate in a situation where a measuring cell with square cross-section is used (the respective calculations are straightforward and are therefore not presented).

Fluorescence emission spectra, $F^{em-sp}(\lambda)$, were detected with constant bandwidth on a wavelength scale. Thus $F^{em-sp}(\lambda)$ represents the spectral density of the fluorescence quantum yield per unit wavelength interval. The following relation allows it to transform $F^{em-sp}(\lambda)$ into $F^{em-sp}(\nu)$:

$$F^{em-sp}(\nu) = (d\nu/d\lambda)^{-1} F^{em-sp}(\lambda) = (-c/\lambda^2) F^{em-sp}(\lambda) \quad (9)$$

Furthermore, for investigating the validity of the Stepanov relation (Eq. (8)), we decided to use an energy scale.

In summary, PS II emission spectra which reflect an exciton equilibrium distribution should follow the relation

$$c_F \cdot F^{em-sp}(E) \cdot \lambda^4 / F^{ex-sp}(E) = e^{-(E-E_{680})/(kT)} \quad (10)$$

with: $E = h\,c/\lambda$; $E_{680} = h\,c/680$ nm; $c_F = [F^{em-sp}(E_{680}) \cdot \lambda^3 / F^{ex-sp}(E_{680})]^{-1}$; T, solvent temperature in K.

In Fig. 3, the logarithm of the left side of Eq. (10) is plotted versus the energy difference $E - E_{680}$. The slope of the straight line in Fig. 3 was not obtained by curve-fitting but calculated according to: $(E - E_{680})/(kT)$ with $T = 295$ K (the room temperature during the measurements). It is obvious that for the whole wavelength range of the chlorophyll Q_y absorption (the abscissa scale of Fig. 3 corresponds to the wavelengths ranging from 700 nm to 645 nm) the validity of Eq. (10) is confirmed.

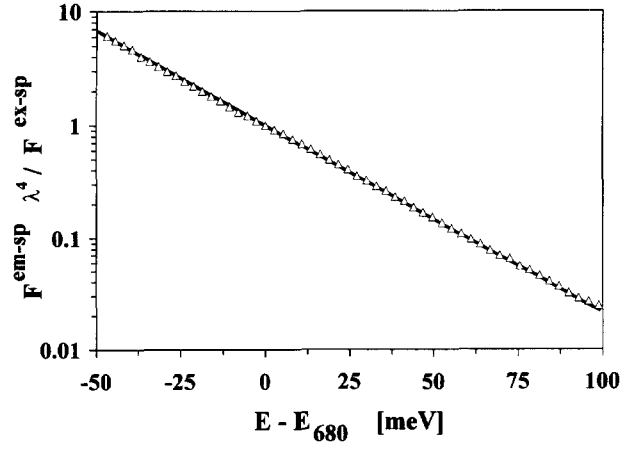

Fig. 3. Relation between emission and excitation spectrum of PS II. The emission spectrum (λ_{ex} = 620 nm) and the excitation spectrum (λ_{em} = 760 nm) used are shown in Fig. 1. The straight line gives Boltzman factor $e^{\Delta E/kT}$ for T = 295 K.

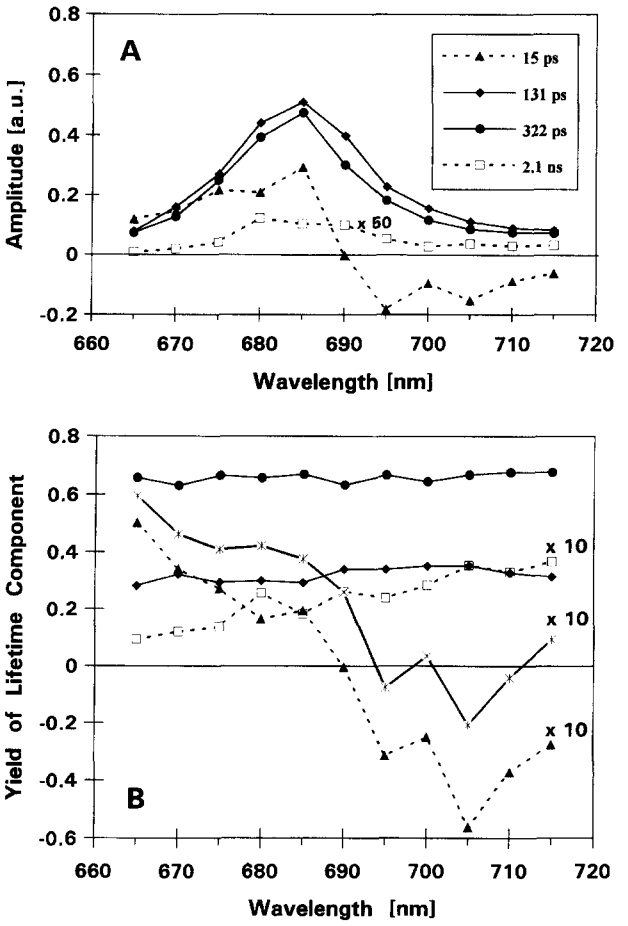

Fig. 4. Decay-associated emission spectrum of PS II particles. Excitation of the rapidly flowing sample (F_0 state) at 645 nm. Decays were fit globally to a sum of four exponentials; the resulting time constants are given in the inset. (A) Amplitudes are plotted as a function of the emission wavelength. For clarity of the graphical presentation, the amplitude of the 2.1 ns component (open squares) is multiplied by a factor of 50. (B) Relative yield of individual lifetime component, $Y_i(\lambda)$. The crosses give the sum of $Y_{15ps}(\lambda)$ and $Y_{2.1ns}(\lambda)$. For the 15 ps component (closed triangles), the 2.1 ns lifetime (open squares) component and their sum (crosses), the relative yield values are multiplied by a factor of 10.

Fluorescence decays after excitation with a picosecond laser pulse were studied in the F_0 state using an excitation wavelength of 645 nm. Decays were measured at eleven emission wavelengths ranging from 665 nm to 715 nm. By using a global data analysis approach with four lifetime components, high-quality fits with χ^2 values between 1.0 and 1.25 were obtained.

In Fig. 4A, the amplitudes as obtained by the four-exponential fit are shown as a function of the emission wavelength (decay-associated spectra). In comparison to the amplitudes of the other lifetime components, the amplitudes of the 2.1 ns component are extremely small, i.e., ~ 0.2% of the sum of A_{131ps} and A_{322ps}. We assume that

this lifetime component is due to a negligibly small amount of impurities. Possible impurities are: 'free' chlorophylls, PS II in the closed reaction-center state, PS I or LHC I contaminations. The enhanced contribution of the 2.1 ns component to the fluorescence emission at longer wavelengths (see Fig. 4B) might indicate the presence of residual PS I or LHC I.

The amplitude spectra of the 131 ps component and the 322 ps component are similar (Fig. 4A, B); differences between these spectra do not exceed the inherent inaccuracies of the curve-fitting approach used. For the 15 ps lifetime component, the occurrence of negative amplitudes at 695 nm and 700 nm is a clear indication for excitation energy transfer from short-wavelength pigments to long-wavelength pigments.

In Fig. 4B, the emission wavelength dependence of the relative yield of the individual lifetime components, $Y_i(\lambda)$, is given. The quantity $Y_i(\lambda)$ gives the contribution of the individual lifetime component to the steady-state fluorescence emission as calculated from the results of the picosecond measurements. The 131 ps and the 322 ps components contribute to the steady-state fluorescence emission by $\sim 35\%$ and $\sim 65\%$, respectively, irrespective of the detection wavelength. (There is a slight increase in the relative yield of the 131 ps and of the 322 ps component with increasing wavelengths. This increase is, at least partially, due to the increasingly negative contribution of the 15 ps component to the sum of the component yields. The sum of the component yields was used to calculate the relative component yields, Y_i, as described in Materials and Methods.) The excitation energy transfer component of 15 ps lifetime creates a positive contribution (increased steady-state fluorescence) of $\sim 5\%$ at 665 nm and a negative contribution (decreased steady-state fluorescence) of $\sim 3.5\%$ at 695 nm. Most likely, Y_{131ps} and Y_{322ps} represent the PS II fluorescence after exciton equilibration has taken place. Thus, Y_{15ps} (excitation energy transfer) and $Y_{2.1ns}$ (impurities) give the deviations of the PS II emission spectrum from the hypothetical spectrum for perfectly rapid exciton equilibration (in percent). In Fig. 4B, the crosses give the sum of $Y_{15ps}(\lambda)$ and $Y_{2.2ns}$. This sum compares well with the fluorescence ratios shown in Fig. 2B, D and E. Common features are a slight decrease in the ratio between 665 and 672 nm (2–5%), a plateau phase between 672 and 682 nm and a further decrease by about 5% between 682 and 695 nm (see Discussion).

4. Discussion

4.1. Definition of rapid exciton equilibration

Laible et al. [17] found by simulations that for their PS I and PS II model rapid energy transfer between chlorophylls leads to rapid establishment of a quasi-equilibrium state in which the fraction of excited state on any antenna chlorophyll (i.e., the excited state residence probability of our terminology), normalized to the total excited state remaining on the model, remains approximately constant. They denote this quasiequilibrium state as 'transfer equilibrium (TE) state'. The meaning of 'transfer equilibrium' is not identical to the meaning of 'exciton equilibrium' because even pronouncedly non-Boltzmann distributions are allowed for the former (arbitrary c_i in Eq. (2)) but not for the latter (c_i close to unity in Eq. (2)). For example, in the PS I model of Laible et al. [17] a TE state is rapidly established, but the excited state residence probabilities exhibit pronounced deviations from a Boltzmann distribution. Thus, the simulations of Laible et al. are suggestive that for PS I the occurrence of the TE state is rapid, but the situation is not appropriately described by the term 'rapid exciton equilibration'. The PS II simulations of Laible et al. [17], however, are suggestive of rapid exciton equilibration.

The occurrence of an exciton equilibrium implies that for $t > \tau_{eq}$, to a first approximation, the relative excited-state residence probability, p_i, depends only on the site energies (E_i), but not on the absolute values of rate constants describing energy transfer and excited state decay (and thus not on the topographical arrangement of antenna chlorophylls and reaction center). Furthermore, for rapid exciton equilibration the fluorescence emission spectrum can be predicted from the absorption spectrum by means of the Stepanov relation without knowledge of the involved site energies. In contrast, for TE states the prediction of the excited state residence probabilities and of emission spectra may require the explicit knowledge of all rate constants involved in the model representation by the Pauli master equation.

In conclusion, 'rapid exciton equilibration' is an important special case of a more general situation which has been denoted as 'rapid occurrence of TE states' [17].

4.2. Occurrence of rapid exciton equilibration

The insensitivity of the emission spectra and excitation spectra with respect to the selection of excitation wavelength and emission wavelength (Figs. 1 and 2), respectively, but also with respect to the state of the trap (open or closed) is in agreement with the assumption that rapid exciton equilibration occurs. In particular, the identity of Stokes and anti-Stokes spectra is best understood under the assumption of rapid thermal equilibration. Nonetheless, these findings alone do not constitute a full proof. The minor deviations from a behavior as predicted for the hypothetical case of '$\tau_{eq} = 0$' are explicable by two alternative hypotheses: (1) there are clear differences in the spectroscopic properties of the pigment groups involved in the (slowest) equilibration process, but the time constant for this process is fast in comparison to the mean lifetime (equilibration is rapid); or (2) there are only very minor differences in the spectroscopic properties of the pigment

groups involved, but the equilibration process is relatively slow (equilibration is not rapid). Furthermore, sample heterogeneities might be involved. The results of time-resolved fluorescence measurements allow us to distinguish between these alternatives.

The time-resolved fluorescence measurements (Fig. 4) demonstrate that the 15 ps time constant is the equilibration time as defined in the context of Eq. (4): seemingly it is the slowest time constant which is due to excitation energy transfer within the PS II antenna system. To a good approximation, the mean excited-state lifetime is given by:

$$\left(A_{131\,\mathrm{ps}} \cdot 131\,\mathrm{ps} + A_{322\,\mathrm{ps}} \cdot 322\,\mathrm{ps}\right)/\left(A_{131\,\mathrm{ps}} + A_{322\,\mathrm{ps}}\right) \sim 240\,\mathrm{ps}. \quad (11)$$

Thus, the equilibration time constant is clearly faster ($\sim$ 16-times faster) than the mean excited-state lifetime; rapid exciton equilibration is achieved.

In intact chloroplasts, upon excitation at 692 nm McCauley et al. [19] observed a 16 ps rise-time component at wavelengths below 690 nm, which is presumably in part due to exciton equilibration within the PS II antenna system. The equilibration time constant of 16 ps observed for intact thylakoids is in good agreement with the equilibration time of 15 ps we observed for PS II membrane particles.

For the time-resolved experiments, the yield of the 15 ps lifetime component (see closed triangles in Fig. 4B) represents the deviations from the hypothetical case of perfectly rapid exciton equilibration ($\tau_{eq} = 0$). For the steady-state experiments, the ratio spectra shown in Fig. 2 are indicative of deviations from perfectly rapid exciton equilibration. As shown in the Appendix (Eq. (A31)), the steady-state ratio spectra (Fig. 2) should exhibit the same spectral dependence as the contribution of the 15 ps lifetime component to the total emission yield (Fig. 4B). Indeed, the spectral dependence and the order of magnitude of the deviations as observable by these two different techniques agree reasonably well (comparison of Fig. 2 emission ratio spectra with closed triangles in Fig. 4B). Slightly better agreement is obtained if the 2.1 ns impurity component is also considered (comparison of Fig. 2 ratio spectra with crosses in Fig. 4B). Thus, two conclusions can be drawn: (1) The results of the time-resolved experiments are consistent with the results obtained by steady-state experiments, and (2) the steady-state ratio spectra of the PS II preparation are determined mainly by the exciton equilibration process; however, a minor contribution due to impurities (e.g., free chlorophylls, residual LHC I) cannot be excluded. It is important to note that, even though the minor impurity component affects the ratio spectra, its contribution to the the steady-state fluorescence spectra itself should be below 4% at all wavelengths considered.

Rapid exciton equilibration implies that the steady-state emission spectrum should be essentially determined by an excited-state equilibrium distribution according to Eq. (2). The prevalence of an exciton equilibrium distribution is not easily testable, because the individual excited state energies and the individual emission spectra of all PS II pigments are unknown. Recently, Jennings and co-workers approached this problem by employing a deconvolution of absorption and emission spectra into asymmetric Gaussian bands and pairwise comparison of absorption-band area with emission-band area [6]. For PS II particles the results obtained did not constitute a fully satisfactory proof for an equilibrium distribution, possibly due to inaccuracies of the light scattering correction and the deconvolution procedure [33]. We investigated the validity of the Stepanov relation. The Stepanov relation for a cluster of inhomogeneously broadened pigments will hold only if rapid exciton equilibration is achieved. Otherwise, significant deviations will occur, as demonstrated by a theoretical study of Van Metter and Knox [34]. (Van Metter and Knox investigated the validity of the Stepanov relation for a single dye species for the case of slow vibrational relaxation; this case is analogous to slow exciton equilibration between the pigments of a pigment cluster.) Fig. 3 demonstrates the validity of the Stepanov relation for the PS II for wavelengths ranging from 645 nm to 700 nm, corresponding to an energy range of almost 6 kT.

In the PS II antenna system rapid energetic (or spectral) equilibration and rapid spatial equilibration occur. This statement is possible because the involved pigment-protein complexes differ to some extent with respect to their spectroscopic properties (see also further below). Preferential excitation of Chl *b* (at large distance from P680) and excitation of long-wavelength chlorophylls (preferentially located in the vicinity of P680) result in the same emission spectra (Fig. 1), which indicates that the excitation at different locations within the PS II antenna system results in the same excited state distribution. Furthermore, the results shown in Fig. 2 are suggestive that the spatial equilibration process, which is reflected in the F_0/F_M ratio spectra of Fig. 2B–D, is identical to the spectral equilibration process, which is reflected in the ratio spectra of Fig. 2E–F and in the yield spectrum of the 15 ps component (Fig. 4B).

At low temperatures (some) energy transfer steps are slowed down. Therefore, it is likely that below a certain temperature, which is still unknown, rapid exciton equilibration does not occur.

The finding that thermal equilibration of excited state energy within the whole PS II antenna system is fast in comparison to the excited state decay by primary charge separation has consequences for our understanding of PS II light-harvesting. For the case of rapid exciton equilibration, the location of different spectral types of pigment does not significantly affect the trapping efficiency. Thus, there is no need to arrange the spectral types of Chl *a* in a way that excitons are funneled to the reaction center (funnel model: the shorter the peak-wavelength, the larger the distance from the reaction center) as demonstrated by

the simulations of Beauregard et al. [35]. In particular, the location of long-wavelength pigments ($\lambda_{peak} > 680$ nm) does not significantly affect the trapping efficiency. This is an argument against a special role of these pigments; presumably, the long-wavelength PS II pigments serve to increase the absorption range of the PS II antenna as already concluded by Trissl [36].

Though often not explicitly stated, rapid exciton equilibration has been the underlying assumption of most models which relate the variable PS II fluorescence with the Q_A redox state (for a recent review see [14]). The experimental proof that rapid exciton equilibration occurs provides an a posteriori justification.

4.3. PS II exciton dynamics

The deviations from the behavior predicted for $\tau_{eq} = 0$ (see Figs. 2 and 4) contribute information about the equilibration process. Based on the experimental results, we propose a model for the PS II equilibration dynamics which accounts for the deviations from perfectly rapid exciton equilibration, as shown in Fig. 5 and outlined below.

We assume that each PS II antenna consists of two groups (or pools) of pigments. The first group, the inner pigment pool, consists of a pigment cluster which includes the reaction center pigment P680. The second group, the peripheral pigment pool, is given either by a single pigment cluster or by several pigment clusters with identical spectroscopic properties which are all direct neighbors of

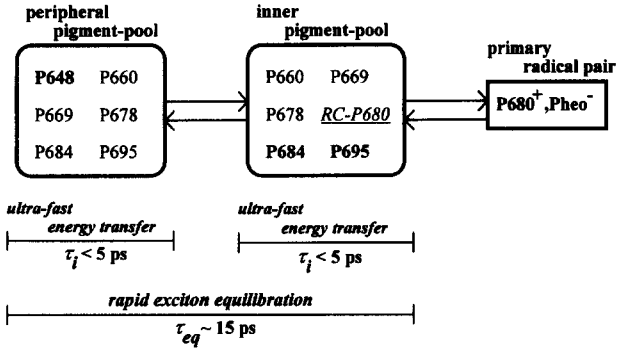

Fig. 5. Schematic representation of the model proposed for the PS II exciton dynamics. Different spectral species of chlorophylls are denoted by a P followed by the peak absorption wavelength obtained by spectral deconvolution [6]; spectral species with an enhanced concentration in the respective pigment pool are printed in bold letters. Excitation energy transfer within the individual pigment pool is characterized by various time constants, τ_i, which are all fast in comparison to the equilibration time constant of 15 ps. The establishment of an exciton equilibrium involving all PS II pigments occurs by excitation energy transfer between the peripheral and the inner pigment pool, a process which is characterized by the equilibration time constant, τ_{eq}, of 15 ps. In the open reaction center state, decay of the excited antenna state results mainly from initiation of primary charge separation (formation of the radical pair [$P680^+/Pheo^-$]); repopulation of the excited antenna state by radical pair recombination is possible.

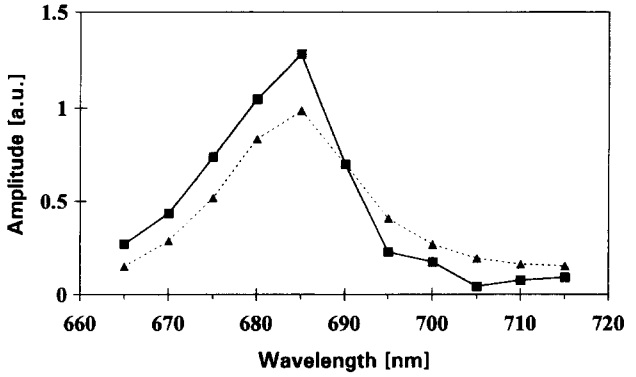

Fig. 6. Fluorescence emission spectra before and after exciton equilibration with $\tau_{eq} = 15$ ps. Closed squares, sum of all amplitudes of the picosecond data-set shown in Fig. 4A ($\lambda_{ex} = 645$ nm); closed triangles, sum of the amplitudes A_{131ps} and A_{322ps}. Under the assumption that processes characterized by time constants faster than 6 ps were not detectable, the sum of the A_i gives the emission spectrum of the initially excited peripheral pigment pool before rapid exciton equilibration with $\tau_{eq} = 15$ ps takes place. The fluorescence emission after exciton equilibration is given by the sum of A_{131ps} and A_{322ps}.

the inner pigment pool. (We assume that it is possible to define a volume around P680 such that all pigments within this volume are part of the inner pigment pool, and all pigments outside of this volume are part of the outer pigment pool. This means that the two pigment pools are spatially distinct.) Both pigment pools, the inner and the peripheral, contain all spectral types of Chl *a*, but the relative concentration of long-wavelength Chl *a* ($\lambda_{abs} > 680$ nm) is enhanced in the inner pigment pool, whereas Chl *b* is found exclusively (or at least in clearly higher concentrations) in the peripheral pigment pool. The exciton dynamics are characterized by three phases.

(I) The absorption event is followed by ultra-fast excitation energy transfer among all pigments of an individual pigment pool; an exciton equilibrium within the pigment pool is reached with time constants ranging from 500 fs to 6 ps. The process of ultra-fast excitation energy transfer is too fast to be detectable by the single-photon timing technique used; its contribution to steady-state spectra is too small to be detectable. For excitation of the peripheral pigment pool by excitation of Chl *b*, the exciton distribution reached by ultra-fast excitation energy transfer is reflected by the emission spectrum shown in Fig. 6 (closed squares).

(II) After ultra-fast excitation energy transfer within the two individual pigment pools, excitation energy transfer between the peripheral pigment pool and the inner pigment pool determines the exciton dynamics. With a time constant of about 15 ps an exciton equilibrium distribution is reached (as discussed above). The resulting fluorescence emission spectrum (see closed triangles in Fig. 6) is clearly different from the emission spectra of the individual pigment pools.

(III) After exciton equilibration among all PS II pigments, the excited state decays with a mean lifetime of 220

ps in the open-reaction center state for the PS II particles investigated. In the open-reaction center state (absence of reduced Q_A), the kinetics of this decay are determined almost exclusively by the charge separation reactions (trap-limited kinetics). This third phase of the PS II exciton dynamics is bi-exponential and can be described by the reversible radical pair model [18] as discussed further below.

The physical identity of the 'peripheral pigment pool' and the 'inner pigment pool' cannot be deduced from the results of this study alone, but some information on their pigment composition can be deduced from the ratio spectra. Eq. (A31) indicates that excitation-spectra ratios (Fig. 2A) reflect the relative contribution of the peripheral pigments to the total excitation spectrum. Thus, in comparison to the inner pigment pool, the peripheral pigment pool is characterized by a clearly higher concentration of Chl *b* absorbing around 650 nm and a moderately higher concentration of chlorophylls absorbing around 678 nm, but by a clearly lower concentration of long-wavelength chlorophylls ($\lambda_{abs} > 680$ nm). Assuming a Stokes shift of 2–4 nm [6], the emission spectra ratios of Fig. 2B, D, E seem to reflect the same pigment distribution as the excitation spectra ratio of Fig. 2A.

The results of this study on the spectral composition of peripheral and inner pigment pool, respectively, can be compared with published results obtained for PS II subparticles or purified pigment/protein complexes. The pigment/protein complexes of the PS II core (CP43 and CP47) do not contain Chl *b* but do contain more long-wavelength pigments than the LHC-polypeptides [6]. The concentration of the 678 nm spectral form of Chl *a* seems to be higher in the LHCII (trimer-forming peripheral LHCs, Lhcb1 and Lhcb2 gene product) than in the PS II core complex [8]. For purified pigment-protein complexes of PS II, Jennings et al. found a wavelength dependence of the emission ratios between LHCs and PS II core pigment-protein complexes which does resemble the results shown in Fig. 2 [33]. Thus, the comparison of the ratio spectra of Fig. 2 with published data is suggestive that the peripheral pigment pool corresponds to the LHCs, whereas the inner pigment pool corresponds to the PS II core-complex. The low-Chl *b* polypeptides (CP24, CP26, CP29), which are not of the LHCII-type, are assumed to be located between the PS II core complex and the LHCII polypeptides [7]. It remains unclear whether the pigments of these minor LHCs are part of the peripheral pigment pool. Also, on the basis of our results we cannot definitely exclude that the inner pigment pool constitutes only part of the PS II core-complex. However, results of Freiberg et al. indicate the absence of excitation energy transfer with time constants as slow as 15 ps in a CP47/D1/D2 preparation [37].

Butler and co-workers suggested that the reaction center pigment, P680, be considered as a separate entity which is not part of the main pigment pool (bipartite model) [38]. The spectral characteristics of the inner pigment pool (e.g., the ratio of excitation spectra as shown in Fig. 2A) exclude the possibility that this pigment pool consists solely of P680.

The occurrence of ultra-fast exciton movement within the peripheral pigment pool is required to explain the emission spectrum shown in Fig. 6 (closed squares), because this emission spectrum cannot result from fluorescence emission of the initially excited Chl *b*. We estimate that all lifetime components with $\tau < \text{fwhm}/10 = 6.5$ ps are undetectable with the experimental set-up used. Thus, exciton dynamics characterized by time constants faster than 6.5 ps determine the (putative) emission spectrum of the peripheral pigment pool shown in Fig. 6. This spectrum seems to be similar to LHCII emission spectra (halfwidth of $\sim$ 16 nm, $F_{peak}/F_{720} \sim 15$, see [33,39]. Eads et al. [40] determined a time constant of ~ 0.5 ps for the exciton movement from Chl *b* to long-wavelength Chl *a* (excitation at 650 nm, emission detected at 690 nm); Kwa et al. [41] found 'spectral equilibration' within the LHCII trimers with time constants of 2–6 ps. All of these experimental findings are in agreement with our proposal that the peripheral pigment pool is given by the LHC pigment-protein complexes and that an exciton equilibrium within the peripheral pigment pool is approached with time constants smaller than 6.5 ps.

A detailed kinetic description of excitation energy transfer within and between pigment-protein complexes could result from application of the Förster theory [4,5]. This has been carried out for C-phycocyanin [42]. However, because the knowledge of all inter-pigment distances and of the spectroscopic properties of each pigment involved is required, presently for PS II this approach is not viable. Alternatively, we propose a description which is based on equilibrium thermodynamics and on the assumption that 'phases' of the exciton dynamics can be distinguished which take place on separable time-scales. This assumption might be unjustified with respect to the separation between first phase (ultra-fast energy transfer within the individual pigment pool) and second phase (rapid exciton equilibration between pigment pools). Possibly, the spectrum shown in Fig. 6 (closed squares) does not represent the equilibrium emission of the peripheral pool but a 'warm' fluorescence resulting from an only partially equilibrated excited-state distribution. Measurements with better time and spectral resolution and more detailed theoretical investigations are required in order to decide whether the assumption of separable time scales results in a serious misconception of the PS II exciton dynamics.

Considering the structural complexity of the PS II protein complex, it might appear problematic to consider only two pigment pools, the peripheral and the inner pigment pool. Indeed, because the 15 ps lifetime component is close to the temporal resolution limit of the experimental set-up used, we cannot definitely exclude that the 15 ps component is composed of two or even more lifetime

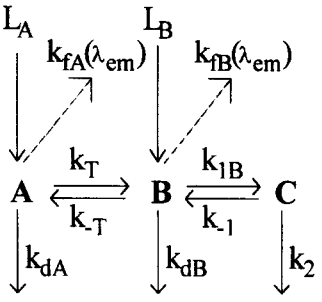

Fig. 7. Rate constants of the two-pigment-pool model with reversible charge separation. L_A and L_B give the rate of photon absorption by the peripheral and the inner pigment pool, respectively. The rate constants for excited state decay, k_{dA} and k_{dB}, include fluorescence decays and non-radiative decays; the rate constant k_2 for decay of the radical pair state includes decay by secondary charge separation, formation of triplets and all non-radiative decay paths not resulting in re-excitation of the PS II antenna. The rate constants k_{fA} and k_{fB} give the probability for fluorescence emission at the wavelength λ_{em}. The rate constants k_T and k_{-T} represent the exciton movement between peripheral pigment pool and inner pigment pool. The rate constant for the transition from the excited state of the inner pigment pool to primary radical-pair state is k_{1B}; the rate constant for the back reaction is k_{-1}.

components. Nonetheless, the presently available experimental results do not provide any clear indication that the two-pool model represents an unjustified simplification.

The results of time-resolved fluorescence studies of other investigators are in agreement with rapid exciton equilibration by exciton movement from peripheral LHCs to the PS II core complex. Mimuro et al. [43] found a shift in the emission peak of PS II-particles at room temperature from ~ 680 nm to ~ 683 nm within 50 ps but no change in the emission spectrum for later times, although surprisingly they did not succeed in resolving a risetime component by curve-fitting. Lin and Knox studied spinach chloroplasts and various *Chlamydomonas reinhardtii* mutants at 77 K [44–46]. They concluded that excitation energy transfer from the LHC to the PS II core complex occurs with time constants of 9 ps and 15 ps for chloroplasts and green algae, respectively [46].

4.4. Mathematical simulations of excited state decay

The bi-exponential decay kinetics observed for PS II particles in the open reaction center state for times $t > 30$ ps is explainable by assuming that the repopulation of the excited antenna state by recombination of the primary radical pair contributes significantly to the prompt fluorescence of PS II (reversible radical pair model [18]) as discussed in more detail elsewhere [12,14]. To account for the tri-exponential picosecond fluorescence results (Fig. 4), it is necessary to extend the RRP model by considering excitation energy transfer processes between a peripheral pigment pool and an inner pigment pool (see Fig. 7).

In Fig. 7, a scheme is shown which illustrates the meaning of the rate constants involved in the mathematical representation of the extended RRP model. The corresponding linear differential equations obtained for low excitation energies – nonlinear phenomena are not considered – are presented in the Appendix (Eqs. (A1)–(A3)).

We tried to determine rate constant values by calculation of amplitudes and time constants which are in agreement with the experimental results. The criteria used for

Table 1
Rate constants, calculated time constants (T_i) and amplitudes (a_i, b_i) for the reversible radical pair model with two pools of antenna pigments

	Experimental results	Fit I	Fit II	Fit III	Approximation
k_T/k_{-T}	–	0.5	1	2	2
k_T (ns^{-1})	–	16.5	30	42	44
k_{1B} (ns^{-1})	–	21.3	11.6	8.2	7.95
k_1^{int} (ns^{-1})	–	738	603	568	552
k_{-1} (ns^{-1})	–	1.252	1.07	1.03	0.96
ΔG_1^{int} (meV)	-	−163	−161	−161	−162
k_2 (ns^{-1})	–	4.12	4.22	4.25	4.20
T_1 (ps)	15	15	15	15	14.5
T_2 (ps)	131	131	131	131	135
T_3 (ps)	322	322	322	322	325
a_1	> +0.5	+0.09	+0.46	+1.19	+1.21
b_1	< −0.5	−0.42	−0.69	−0.78	−0.78
a_2	~ 0.55	0.600	0.572	0.565	0.562
b_2	~ 0.55	0.501	0.527	0.534	0.535
a_2^{avg}	~ 0.55	0.550	0.550	0.550	0.548
$\delta a_2/a_2^{avg}$	–	18%	8.2%	5.6%	4.9%

For definition of rate constants see Fig. 7. The intrinsic rate constant of primary charge separation was calculated according to: $k_1^{int} = (N/c_E)\ k_T\ (k_T + k_{-T})^{-1}\ k_{1B}$ with N (number of Chl a) and c_E (energy concentration factor) equal to 140 and 1.35, respectively [25]; $\Delta G_1^{int} = 25.5$ meV $\ln(k_{-1}/k_1^{int})$. a_i and b_i are the calculated amplitudes for the excited state decay of the outer and inner pigment pool, respectively (normalization such that $a_2 + a_3 = b_2 + b_3 = 1$); a_2^{avg} is the mean value of a_2 and b_2; $\delta\ a_2$ is the difference between a_2 and b_2. Columns denoted with Fit I, Fit II and Fit III: for a fixed k_T/k_{-T} ratio, rate constants were chosen which result in time constants and amplitudes similiar to the experimental results. Last column: the rate constants result from the approximation derived in the Appendix.

judging whether there is agreement between calculated kinetic parameters (A_i, B_i and T_i) and experimental results are presented in the second column of Table 1. Upon excitation at 645 nm predominantly Chl *b* is excited which is presumably located exclusively in the outer pigment pool. Therefore, we assumed that 85% of the 645 nm photons are absorbed by pigments of the outer pigment pool. The rate constants for excited state decay by fluorescence emission and thermal deacitvation are not critical for the results of the calculations unless unreasonably high values are used; it is assumed: $k_{dA} = k_{dB} = 0.3$ ns^{-1} [21,25].

Agreement between calculation and experimental results could be achieved only for k_T/k_{-T} greater than unity (Fit III). For k_T/k_{-T} smaller than or equal to unity (Fit I and Fit II) the absolute values of the amplitudes a_1 and b_1 are smaller than the required limits. Moreover, there are pronounced deviations between a_2 and b_2 for $k_T/k_{-T} = 0.5$.

In the Appendix it is described how an approximate solution of the differential Eqs. (A1)–(A3) can be obtained. The proposed approximation (Eq. A5) allows a mathematical separation of equilibration kinetics (Eq. (A8)) and charge separation kinetics (Eqs. (A16), (A17)). Using this approximation, rate constants were calculated directly from the experimental results using the rationale described in the Appendix (Eqs. (A8)–(A19)) for $k_T/k_{-T} = 2$; they are given in the upper part of Table 1, last column. The rate constants obtained by means of the approximate solution agree reasonably well (deviations of 1.2% to 6.8%) with the ones given in the column denoted as Fit III. It should be noted that this agreement is not a trivial consequence of $T_1 < T_2$; for $k_T/k_{-T} < 1$ (Fit I in Table 1): a comparison of charge separation rate constants of the exact solution with the ones of the approximate solution reveals considerable differences.

For all three fits, a_2^{avg} and all time constant values agree perfectly with the experimental results. Consequently, for all three fits the apparent equilibration time constant T_1 (always 15 ps) is clearly faster than the mean excited state lifetime (always 240 ps). However, Fit I corresponds to a situation which cannot be denoted as rapid exciton equilibration because, for $t \gg T_1$, the relative exciton population of the inner pigment pool as compared to the outer pigment pool is not approximately time independent (difference between a_2 and b_2 of 18%, last line of Table 1). Thus, the finding that the (slowest) rise-time component is clearly faster than the mean excited state lifetime does not necessarily indicate the occurrence of rapid exciton equilibration.

In conclusion, the simulation results summarized in Table 1 indicate: (1) at present the values of the model parameters k_T and k_{-T} cannot be determined unambiguously; (2) agreement with the experimental results is obtained only for $k_T/k_{-T} > 1$; (3) the finding that the (slowest) rise-time component is clearly faster than the mean excited state lifetime is not sufficient to prove the occurrence of rapid exciton equilibration; (4) the finding that the (slowest) rise-time component is clearly faster than the mean excited state lifetime does not necessarily indicate the applicability of the approximation derived in the Appendix (i.e., the applicability of the conventional RRP model); (5) however, the approximation derived in the Appendix is reasonably good for the actual PS II, and by means of this approximation we can determine values for the charge separations rate constants k_1, k_{-1} and k_2 (but not for k_T and k_{-T}).

We estimate the k_T/k_{-T} ratio to be between 1 and 2 (Table 1). Jennings et al. [8] estimate that, in the case of an exciton equilibrium, the probability of the excited state to reside on chlorophylls of the LHCII is about 50%. Assuming that all LHCII of the PS II constitute the outer pigment pool, this number is suggestive of an k_T/k_{-T} ratio of about one, a value which we consider to be not in serious conflict with our estimate.

In several recent studies the RRP model was used to deduce charge separation rate constants from picosecond fluorescence data [21,25,48]. In all of these studies the influence of the exciton equilibration kinetics on slower kinetic components was neglected; charge separation rate constants were calculated under the assumption that the approximation derived in the Appendix (Eqs. (A5) to (A19)) is reasonable. The simulation results summarized in Table 1 indicate that this approach is justified for the intact PS II of higher plants.

4.5. Charge separation rate constants

Surprisingly, all charge separation rate constants given in Table 1 (Fit III) are somewhat faster than the corresponding values obtained for PS II of intact thylakoids [21,25]. This result reflects the finding that the time constants found in PS II membrane particles (see Fig. 4 and [15,16]) are faster than the time constants of intact thylakoids which are usually assigned to PS II (see review articles [11–14]). At present we cannot offer an explanation for this observation.

The rate constants k_1 and k_{-1} of the reversible radical-pair model describe the transition between two states of PS II: (1) the excited antenna state and (2) the primary radical-pair state. For rapid exciton equilibration, k_1 is determined by the product of k_1^{int}, the intrinsic rate constant of primary charge separation which describes the reaction: $P680^* -> [P680^+, Pheo^-]$, and of P_{680}, the probability of the excited state to reside on P680. Thus, calculation of k_1^{int} should be possible according to

$$k_1^{int} = k_1/P_{680} \quad (12)$$

However, Eq. (12) relies on two debatable assumptions as discussed in the following.

(i) Our experimental results do not provide any indication that there are PS II pigments with non-Boltzmann

excited-state residence probabilities leading to c_i values in Eq. (2) which deviate clearly from unity. Nonetheless, we cannot exclude that one or a few such pigments are present in the PS II antenna system; their contribution to spectra might be too small to be detectable. For P680, c_{P680} values in Eq. (2) which are clearly smaller than unity would be possible in case the excitation energy transfer to P680 and away from P680 were not fast in comparison to $(k_1^{int})^{-1}$. However, recent investigations on isolated PS II reaction centers are suggestive of ultra-fast excitation energy transfer involving P680 [49]. Furthermore, the observed effect of Q_A reduction on k_1 [18,21,48] can only be reconciled with slow energy transfer steps between bulk antenna and P680 if a pronounced effect of the Q_A redox state on energy transfer steps is assumed to occur; something we consider to be unlikely.

(ii) For calculation of k_1^{int} we assumed that the site energy of P680 (E_{680} in Eq. (2)) can be estimated from its putative absorption maximum at 680 nm. This assumption is questionable for P680. Possibly P680 is an excitonically coupled pigment dimer (or multimer). Therefore, the existence of excited P680 states which cannot be reached by an optical transition but which are in thermal equilibrium with optically populated excited states cannot be excluded. Such states could result in a significant entropic contribution to E_{680} which is not included in the E_{680} estimate based on the P680 absorption maximum.

Comparison of our k_1^{int} with time constants determined for the formation of the primary radical pair in isolated PS II reaction [50,51] is problematic because our value as well as the reaction center values are uncertain due to the above-mentioned unresolved questions (i and ii).

Previously we compared electric field-induced relative changes of k_1^{int} with electron transfer theories [25]. The magnitude of such relative changes does not depend on the (uncertain) value of E_{680}.

4.6. Summary

In case of rapid exciton equilibration, the charge separation efficiency and many spectroscopic properties of the antenna system are determined by an excited state equilibrium distribution, but not by kinetic details of excitation energy transfer. In the plant PS II (consisting of core complex plus full LHC system) at room temperature, an excited state equilibrium distribution is rapidly established; rapid exciton equilibration occurs. The validity of the Stepanov relation indicates that the equilibrium distribution is close to a Boltzmann distribution. It remains an open question, whether rapid exciton equilibration occurs also in other photosystems.

Deviations (of about 10%) from the behavior predicted for perfectly rapid exciton equilibration are detectable in steady-state spectra and in time-resolved fluorescence decays. These deviations (and all other experimental results of this study) are accounted for by a phenomenological model involving an outer pigment pool (LHC complexes), an inner pigment pool (core complex) and the reversibility of the primary charge separation reaction. Simulations demonstrate that application of this model results in essentially the same values for charge separation rate constants as application of the frequently used reversible radical pair model.

Acknowledgements

This research was supported by the Director, Office of Energy Research, Office of Basic Energy Sciences, Energy Biosciences Division of the U.S. Dept. of Energy under contract DE-AC03-76SF00098. We thank Prof. R. Knox (Rochester, USA) for helpful discussions. H.D. would like to thank Prof. H. Senger (Marburg, Germany) for his support and encouragement. A Feodor Lynen fellowship of the Alexander von Humboldt-Stiftung (to H.D.) and support by the Deutsche Forschungsgemeinschaft (SFB 305, Projekt B1) are gratefully acknowledged.

Appendix A

Three states are explicitly considered: [A], the exciton resides in the peripheral pigment pool; [B], the exciton resides in the inner pigment pool; and [C], the primary radical pair state. *A(t)*, *B(t)* and *C(t)* give the probability for the system to be in state [A], [B] or [C], respectively. The (transition) rate constants for transitions between states are defined as shown in Fig. 7.

The dynamics of the system shown in Fig. 7 are described by the following set of linear differential equations:

$$dA/dt = -(k_T + k_{dA})A + k_{-T}B + L_A \quad (A1)$$

$$dB/dt = -(k_{-T} + k_{1B} + k_{dB})B + k_T A + k_{-1}C + L_B \quad (A2)$$

$$dC/dt = -(k_{-1} + k_2)C + k_{1B}B \quad (A3)$$

L_A and L_B give the rate of excited state population of the peripheral pigment pool and the inner pigment pool, respectively. For treatment of the picosecond fluorescence results, L_A and L_B are assumed to be δ-functions (of time). For treatment of steady-state experiments, L_A and L_B are time-independent. For light of a given photon flux density, L_A and L_B depend on the wavelength of the excitation light; the ratio between L_A/L_B at the wavelength λ_{ex} is given by the ratio between the absorption of the inner pigment pool and the absorption of the peripheral pigment pool.

The fluorescence emission at the wavelength λ_{em} is given by

$$F(t, \lambda_{em}) = k_{fA}(\lambda_{em})A(t) + k_{fB}(\lambda_{em})B(t) \quad (A4)$$

For excitation with infinitely short light pulses (δ-pulse excitation), this system of differential equations predicts tri-exponential kinetics. An exact analytical solution can be obtained by standard techniques for treating linear differential equations; however, the values of the time constants and amplitudes obtained are highly complicated functions of all rate constants involved. More insight into the relation between rate constants and observable kinetic parameters provides an approximate solution, obtained under the assumption:

$$k_T,\ k_{-T} \gg k_{dA},\ k_{dB},\ k_{1B}. \tag{A5}$$

Assuming that (A5) is valid, we can treat the equilibration process under the assumption:

$$A(t) + B(t) = L_0 \quad \text{or} \quad A(t) = L_0 - B(t) \tag{A6}$$

with

$$L_0 = A_0(\lambda_{ex}) + B_0(\lambda_{ex}) \tag{A7}$$

where $A_0(\lambda_{ex})$ and $B_0(\lambda_{ex})$ give the probability for the peripheral pigment pool and the inner-pigment pool, respectively, to be initially excited by the light pulse.

Using Eq. (A6), Eq. (A1) can be written as

$$dA/dt = -k_T\, A + k_{-T}(L_0 - A). \tag{A8}$$

The solution for δ-pulse excitation is given by

$$A(t) = A_{eq} + \{A_0 - A_{eq}\}\, e^{(-t/\tau_{eq})} \tag{A9}$$

and

$$B(t) = B_{eq} + \{B_0 - B_{eq}\}\, e^{(-t/\tau_{eq})} \tag{A10}$$

with

$$\tau_{eq} = 1/(k_T + k_{-T}), \tag{A11}$$

$$A_{eq} = L_0\{k_{-T}/(k_T + k_{-T})\} \tag{A12}$$

and

$$B_{eq} = L_0\{k_T/(k_T + k_{-T})\}. \tag{A13}$$

The Eqs. (A9) and (A10) describe the equilibration kinetics. After excition equlibration has taken place, A and B are given by

$$A(t) = \{A(t) + B(t)\}\{k_{-T}/(k_T + k_{-T})\} \tag{A14}$$

and

$$B(t) = \{A(t) + B(t)\}\{k_T/(k_T + k_{-T})\}. \tag{A15}$$

Addition of Eqs. (A1) and (A2) and substitution of A and B according to (A14) and (A15), respectively, yields

$$d(A + B)/dt = -(k_1 + k_A)(A + B) + k_{-1}C + L_0 \tag{A16}$$

$$dC/dt = -(k_{-1} + k_2)C + k_1(A + B) \tag{A17}$$

with

$$k_1 = k_{1B}k_T/(k_T + k_{-T}) \tag{A18}$$

and

$$k_A = k_{dA}k_{-T}/(k_T + k_{-T}) + k_{dB}k_T/(k_T + k_{-T}). \tag{A19}$$

Eqs. (A16) and (A17) are identical to the differential equations of the RRP model given elsewhere [18,25,48]. Eqs. (A18) and (A19) give the relations between the rate constants of the RRP model and the rate constants of the two pigment pool model with reversible charge separation as shown in Fig. 7.

To facilitate the interpretation of the steady-state fluorescence ratio spectra shown in Fig. 2, the steady-state solution of the differential Eqs. (A1)–(A3) is presented. The steady-state solution is obtained for $dA/dt = dB/dt = dC/dt = 0$; L_A and L_B give the rate of photon absorption by the peripheral pigment pool and the inner pigment pool, respectively (in: absorption events/s). By some straightforward transformations we obtain for the steady-state values of A and B:

$$A^{ss} = \{(L_A + L_B)k_{-T} + (k_{dB} + k_{pB})L_A\}/d \tag{A20}$$

and

$$B^{ss} = \{(L_A + L_B)k_T + k_{dA}L_B\}/d \tag{A21}$$

with

$$k_{pB} = k_{1B}k_2/(k_{-1} + k_2) \tag{A22}$$

and

$$d = k_{dA}k_{-T} + (k_{dB} + k_{pB})k_T + (k_{dB} + k_{pB})k_{dA}. \tag{A23}$$

Trap-closure by Q_A reduction results in a decrease of k_{pB}, whereas k_T, k_{-T}, k_{dA} and k_{dB} are assumed to be unaffected.

Based on (A20) and (A21), calculation of the steady-state fluorescence emission, $F(\lambda_{em}, \lambda_{ex})$, according to Eq. (A4) yields

$$F(\lambda_{em}, \lambda_{ex}) = F_{eq} + F_{dev} \tag{A24}$$

with

$$F_{eq}(\lambda_{em}, \lambda_{ex}) = \{(L_A(\lambda_{ex}) + L_B(\lambda_{ex}))\{k_{fA}(\lambda_{em})k_{-T} + k_{fB}(\lambda_{em})k_T\}/d \tag{A25}$$

and

$$F_{dev}(\lambda_{em}, \lambda_{ex}) = \{L_A(\lambda_{ex})k_{fA}(\lambda_{em})(k_{dB} + k_{pB}) + L_B(\lambda_{ex})k_{fB}(\lambda_{em})k_{dA}\}/d \tag{A26}$$

(The denominator, d, in (A25) and (A26) is given by (A23).) F_{eq} gives the fluorescence emission for infinitely fast exciton equilibration; F_{dev} gives the deviations from F_{eq} which are due to the not-infinitely fast equilibration process.

Eq. (A25) predicts an emission spectrum for F_{eq} which is independent of which pigment was initially excited, i.e., an emission spectrum independent of the excitation wavelength; the excitation spectrum is predicted to be identical to the sum of the absorption spectra of the peripheral pigment pool and that of the inner pigment pool. Also, the emission and excitation spectra of the F_{eq} contribution to the fluorescence emission do not depend on k_{pB} and therefore not on the extent of PS II trap closure.

To avoid unnecessarily complicated equations in the following two approximations are used: first, for the relation between (F_{dev}/F_{eq}) of the F_0 state and of the F_M state

$$F_{dev,M}/F_{eq,M} < F_{dev,0}/F_{eq,0}. \quad (A28)$$

and second, in the F_0-state $k_{pB} >> k_{dA}$, k_{dB} and therefore

$$F_{dev,0} = k_{pB} L_A k_{fA}/d. \quad (A29)$$

(Based on the reasonable assumption that $k_{pB,0} \gg k_{pB,M}$, the relation (A28) is obtained by using the ratio of Eqs. (A26) and (A25) for the F_M and F_0 states.)

Using the first approximation (Eq. (A28)), we obtain for the F_0/F_M ratio

$$F_0/F_M = (F_{eq,0} + F_{dev,0})/F_{eq,M}$$
$$= (F_{eq,0}/F_{eq,M})(1 + F_{dev,0}/F_{eq,0}) \quad (A30)$$

Thus, the deviations of the F_0/F_M ratio spectra from a straight line in parallel to the wavelength axis are given by $F_{dev,0}/F_{eq,0}$. By using Eq. (A29) we obtain

$$F_{dev,0}/F_{eq,0} = \{k_{pB}/(k_T + k_{-T})\} \cdot \{S_{em,A}(\lambda_{em})/S_{em,eq}(\lambda_{em})\} \cdot \{S_{ex,A}(\lambda_{ex})/S_{ex,eq}(\lambda_{ex}\} \quad (A31)$$

with

$$S_{em,A}(\lambda_{em}) = k_{fA}(\lambda_{em}), \quad (A32)$$

$$S_{em,eq}(\lambda_{em}) = k_{fA}(\lambda_{em})\, k_{-T}/(k_T + k_{-T}) + k_{fB}(\lambda_{em})\, k_T/(k_T + k_{-T}), \quad (A33)$$

$$S_{ex,A}(\lambda_{ex}) = L_A(\lambda_{ex}),$$

and

$$S_{ex,eq}(\lambda_{ex}) = (L_A(\lambda_{ex}) + L_B(\lambda_{ex})). \quad (A34)$$

According to Eq. (A31), the deviations of emission-spectra ratios (as shown in Fig. 2) from a straight line correspond to the relative contribution of the peripheral pigment pool to the emission spectrum at the particular wavelength. In analogy, the deviations of excitation-spectra ratios correspond to the relative contribution of the peripheral pigment pool to the excitation (or absorption) spectrum.

References

[1] Lam, E., Baltimore, B., Ortiz, W., Chollar, S., Melis, A. and Malkin, R. (1983) Biochim. Biophys. Acta 724, 201–211.
[2] Bassi, R.B., Dainese, P. and Marquardt, J. (1993) Eur. J. Biochem. 212, 297–303.
[3] Knox, R.S. (1977) in Primary Processes of Photosynthesis (Barber, J., ed.), pp. 55–97, Elsevier, Amsterdam.
[4] Förster, T. (1948) Ann. Phys. (Leipzig) 2, 55–75.
[5] Förster, T. (1949) Z. Naturforsch. A4, 321–327.
[6] Zucchelli, G., Jennings, R.C. and Garlaschi, F.M. (1992) Biochim. Biophys. Acta 1099, 163–169.
[7] Jansson, S. (1994) Biochim. Biophys. Acta 1184, 1–19.
[8] Jennings, R.C., Bassi, R., Garlaschi, F.M., Dainese, P. and Zucchelli, G. (1993) Biochemistry 32, 3202–3210.
[9] Kühlbrandt, W. and Wang, D.N. (1991) Nature 350, 130–134.
[10] Kühlbrandt, W., Wang, D.N. and Fujiyoshi, Y. (1994) Nature 367, 614–621.
[11] Van Grondelle, R., Dekker, J.P., Gilbro, T. and Sundstrom, V. (1994) Biochim. Biophys. Acta 1187, 1–65.
[12] Holzwarth, A.R. and Roelofs, T.A. (1992) J. Photochem. Photobiol. B15, 45–62.
[13] Renger, G. (1992) in The Photosystems: Structure, Function and Molecular Biology (Barber, J., ed.), pp. 45–99, Elsevier, Amsterdam.
[14] Dau, H. (1994) Photochem. Photobiol. 60, 1–23.
[15] Hodges, M. and Moya, I. (1987) Biochim. Biophys. Acta 892, 42–47.
[16] Van Mieghem, F.J.E., Searle, G.F.W., Rutherford, A.W. and Schaafsma, T.J. (1992) Biochim. Biophys. Acta 1100, 198–206.
[17] Laible, P.D., Zipfel, W. and Owens, T.G. (1994) Biophys. J. 66, 844–860.
[18] Schatz, G.H., Brock, H. and Holzwarth, A.R. (1988) Biophys. J. 54, 397–405.
[19] McCauley, S.W., Bittersmann, E. and Holzwarth, A.R. (1989) FEBS Lett. 249, 285–288.
[20] McCauley, S.W., Bittersmann, E., Müller, M.G. and Holzwarth, A.R. (1990) in Current Research in Photosynthesis, Vol. II (Baltscheffsky, M., ed.), pp. 297–300, Kluwer, Dordrecht.
[21] Roelofs, T.A., Lee, C.-H. and Holzwarth, A.R. (1992) Biophys. J. 61, 1147–1163.
[22] Van Grondelle, R. (1985) Biochim. Biophys. Acta 811, 147–195.
[23] Dau, H., Andrews, J.C., Roelofs, T.A., Latimer, M.J., Liang, W., Yachandra, V.K., Sauer, K. and Klein, M.P. (1995) Biochemistry 34, 5274–5287.
[24] Dau, H. and Sauer, K. (1991) Biochim. Biophys. Acta 1089, 49–60.
[25] Dau, H. and Sauer, K. (1992) Biochim. Biophys. Acta 1142, 311–320.
[26] Mukerji, I and Sauer, K. (1993) Biochim. Biophys. Acta 1142, 311–320.
[27] Wendler, J., John, W., Scheer, H. and Holzwarth, A.R. (1986) Photochem. Photobiol. 44, 79–85.
[28] Knutson, J.R., Beechem, J.M. and Brand, L. (1983) Chem. Phys. Lett. 102, 501–507.
[29] Jennings, R.C., Zucchelli, G. and Garlaschi, F.M. (1990) Biochim. Biophys. Acta 1016, 259–265.
[30] Jennings, R.C., Zucchelli, G. and Garlaschi, F.M. (1991) Biochim. Biophys. Acta 1060, 245–250.
[31] Stepanov, B.I. (1957) Sov. Phys. Dokl. 2, 81–84.
[32] Neporent, B.S. (1958) Sov. Phys. Dokl. 3, 337–340.
[33] Jennings, R.C., Garlaschi, F.M., Bassi, R., Zucchelli, G., Vianelli, A. and Dainese, P. (1993) Biochim. Biophys. Acta 1183, 194–200.
[34] Van Metter, R.L. and Knox, R.S. (1976) Chem. Phys. 12, 333–340.
[35] Beauregard, M., Martin, I. and Holzwarth, A.R. (1991) Biochim. Biophys. Acta 1060, 271–283.
[36] Trissl, H. (1993) Photosynth. Res. 35, 247–263.
[37] Freiberg, A., Timpmann, K., Moskalenko, A.A. and Kuznetsova, N.Y. (1994) Biochim. Biophys. Acta 1184, 45–53.
[38] Butler, W.L. (1978) Annu. Rev. Plant Physiol. 29, 345–378.
[39] Hemelrijk, P.W., Kwa, L.S., Van Grondelle, R. and Dekker, J.P. (1992) Biochim. Biophys. Acta 1098, 159–166.
[40] Eads, D.D., Castner Jr., E.W., Alberte, R.S., Mets, L. and Fleming, G.R. (1989) J. Phys. Chem. 93, 8271–8275.
[41] Kwa, S.L.S., Van Amerongen, H., Lin, S., Dekker, J.P., Van Grondelle, R. and Struve, W.S. (1992) Biochim. Biophys. Acta 1102, 202–212.
[42] Sauer, K. and Scheer, H. (1988) Biochim. Biophys. Acta 936, 157–170.

[43] Mimuro, M., Yamazaki, I., Tamai, N., Yamazaki, T. and Fujita, Y. (1987) in Primary Processes in Photobiology (Kobayashi, ed.), pp. 23–32, Springer, Berlin.
[44] Knox, R.S. and Lin, S. (1988) in Photosynthetic Light Harvesting Systems: Structure and Function (Scheer, H. and Schneider, S., eds.), pp. 567–577, De Gruyter, Berlin.
[45] Lin, S. and Knox, R.S. (1988) J. Luminesc. 40/41, 209–210.
[46] Lin, S. and Knox, R.S. (1991) Photosynth. Res. 27, 157–168.
[48] Leibl, W., Breton, J., Deprez, J. and Trissl, H.-W.(1989) Photosynth. Res. 22, 33–36.
[49] Durrant, A.U., Hastings, G., Joseph, D.M., Barber, J., Porter, G. and Klug, D.R. (1992) Proc. Natl. Acad. Sci. USA 89, 11632–11636.
[50] Wasielewski, M.R., Johnson, D.G., Seibert, M. and Govindjee (1989) Proc. Natl. Acad. Sci. USA 86, 524–528.
[51] Durrant, A.U., Hastings, G., Joseph, D.M., Barber, J., Porter, G. and Klug, D.R. (1993) Biochemistry 32, 8259–8267.